coatings

MDPI

Article

Investigating the Synergic Effects of WS_2 and ECAP on Degradation Behavior of AZ91 Magnesium Alloy

Aqeel Abbas [1] and Song-Jeng Huang [2,*]

[1] Interdisciplanary Research Center, King Fahad University of Petroleum and Minerals, Dhahran 31261, Saudi Arabia
[2] Department of Mechanical Engineering, National Taiwan University of Science and Technology, Taipei 10607, Taiwan
* Correspondence: sgjghuang@mail.ntust.edu.tw

Abstract: In this research, WS_2/AZ91 metal matrix composites were manufactured using the stir casting method. The composites were severely deformed using equal channel angular pressing (ECAP). The degradation behavior of severely deformed and as-cast samples was investigated using the three-electrode system in a 3.5 wt% NaCl solution. The corrosion products and surface morphology of the corroded surfaces were investigated using an x-ray diffractometer and scanning electron microscopy. The results revealed that as-cast monolithic AZ91 exhibited the highest corrosion potential of (−1.553 mV) and a minimum degradation rate (4.099 $m{\cdot}a^{-1}$). The reduction ion grain size after severe plastic deformation increased the degradability of WS_2/AZ91 composites. Severe plastic deformation reduced the grain size, which led to an increase in the corrosion rate. The synergic effects of (tungsten disulfide) WS_2 and ECAP increased the degradation rate to (4.59 $m{\cdot}a^{-1}$) in two-pass 1 wt% WS_2/AZ91. The increase in WS_2 contents decreased the degradation rate (4.512 $m{\cdot}a^{-1}$) in homogenized 1 wt% WS_2/AZ91 composites. The degradability of AZ91 increased in all conditions under the synergic effects of WS_2 and severe plastic deformation. Magnesium and magnesium hydroxide were observed as corrosion products. The maximum surface roughness in two-pass 1 wt% WS_2/AZ91 indicated the highest material removed by corrosion from the surface of the composites.

Keywords: WS_2/AZ91; degradation/corrosion behavior; ECAP; Tafel curves; potentiodynamic polarization

Citation: Abbas, A.; Huang, S.-J. Investigating the Synergic Effects of WS_2 and ECAP on Degradation Behavior of AZ91 Magnesium Alloy. *Coatings* **2022**, *12*, 1710. https://doi.org/10.3390/coatings12111710

Academic Editor: Alina Vladescu

Received: 4 September 2022
Accepted: 24 October 2022
Published: 9 November 2022

1. Introduction

Magnesium is one of the lightest structural metals and can replace conventional aluminum alloys in the automotive and aerospace industries [1]. Magnesium alloys have a low density, high specific rigidity, and excellent electromagnetic shielding performance [2]. Magnesium is a biocompatible material and has many applications in biomedical implants. The degradable behavior and biocompatibility of magnesium make it most suitable for biomedical application in order to avoid second surgery [3]. It requires certain mechanical properties and controlled degradation properties for effective use in biomedical applications. However, a poor corrosion resistance and less specific strength of magnesium alloys have become a bottleneck that restrict their applications [4]. The degradation behavior and specific strength of the magnesium can be controlled by the development of metal matrix composites [5]. The reinforcement type, composition, dispersion, and secondary phases produced have significant effects on controlling the degradation behavior of the magnesium-based metal matrix composites [6]. The reinforcement additives in magnesium play a comprehensive role in forming the solid solution of intermetallic compounds to protect from oxides. The addition of ceramics, aluminum, SiC, V, Ag, Ni, and Zn are the major elements used to improve magnesium's corrosion resistance [7]. The severe plastic deformation and heat treatment alter the microstructure, which consequently affects

the mechanical and degradation behavior of composites. WS_2 is excellent reinforcement for strength enhancement since it is also well established that tungsten and sulfur have significant effects on the degradation behavior of magnesium alloys. Therefore, WS_2 was selected as reinforcement to investigate the degradation behavior of AZ91 magnesium alloy [8–10].

Stir casting techniques used to manufacture the metal matrix composites have been considered as one of the basic methods because of their homogeneous and uniform dispersion of additives with less porosity [6]. The formation of intermetallic compounds is the key phenomenon in the casting process [11]. The degradation behavior of the magnesium alloys and composites is significantly affected by the distribution and morphology of intermetallics. The intermetallics are required to be dissolved using heat treatments and SPD. The intermetallic compounds are dissolved during the homogenization process, and ductility is improved. The grain size is reduced during severe plastic deformation, which consequently affects the degradation rate [12,13]. It has been proven that grain refinement is one of the most efficient ways to improve mechanical strength and promote uniform degradation behavior due to a homogeneous phase distribution. Several studies have been performed to investigate the effects of SPD on the degradation behavior of magnesium alloys [14,15]. Equal channel angular pressing (ECAP) is an advanced technique used to perform severe plastic deformation. ECAP reduces the crystalline defects and improves the grain boundary density [16]. SPD has increased the mechanical strength and has had the opposite effect on corrosion properties. It accelerates the degradation rate, which is due to a high dislocation density and insufficient recrystallization. The degradation rate is also increased due to the surface energy and residual stresses produced after SPD [17]. Mg and alloys are prominent in biomedical applications because of their biodegradable behavior. The WS_2 has the ability to improve mechanical properties at higher temperatures and pressure. The property of self-lubricating and forming the passivation layer on the surface enhances the tribological and corrosion resistance of the matrix alloys. The effects of WS_2 concentration, heat treatments, and severe plastic deformation via ECAP on the mechanical behavior of AZ91 were investigated in our previous research [8,10,18]. The excellent mechanical properties were observed after heat treatment and ECAP processing. Several investigations have been conducted on the corrosion behavior of Mg alloys by different additives. To the best of our knowledge, no one has tried to investigate the synergic effects of both severe plastic deformation and tungsten disulfide. There are very limited data available about the degradation behavior of AZ91 under synergic effects. Investigating the degradable behavior of a prepared composite has been planned.

In this research, magnesium alloy AZ91 reinforced with different concentrations of WS_2 was manufactured via the stir casting method. The composites were homogenized and severely deformed by subsequently using ECAP. The effects of WS_2 concentration and SPD on the degradation behavior of AZ91 in 3.5 wt% NaCl solution were analyzed.

2. Materials and Method

Composites with different concentrations (0, 0.6, 1) wt% of WS_2 were manufactured using a stir casting furnace under the protective environment of argon. The matrix (AZ91) and reinforcement were heated to 800 °C and then stirred at 400 RPM for 5 min for uniform and homogenous mixing. The composite ingots were cooled at room temperature [7]. The composites were homogenized at 410 °C for 24 h and then quenched in plain water for 3 s. The severe plastic deformation of the samples was performed via ECAP with an internal die angle of 120° using route B_C. The complete severe plastic deformation process can also be found in the previous research work [18]. All samples were polished using ASTM-E8 metallographic techniques to make the surface smooth.

The electrochemical behavior of the composites was investigated using potentiostat (Multi Autolab/M204, Metrohm, Zofingen, Switzerland) apparatus, as shown in Figure 1. The standard three-electrode cells were composed of the sample as a working electrode, platinum plate as a counter electrode, and saturated calomel (Ag/AgCl) as a reference

electrode. The 3.5 wt% NaCl solution was used as an electrolyte, and the 1.76 cm^2 area of the sample was exposed to the electrolyte. The open-circuit potential (OCP) was recorded after immersion of the electrode in the solution for 1 h (vs. Ag/AgCl). The potentiodynamic current–potential curves (Tafel curves) were recorded from −2 V to +0.2 V at a scan rate of 0.5 mV/min. The samples were cleaned with deionized water and dried in the air. To achieve better compliance between the curves, at least three specimens of each sample were tested. However, only one suitable specimen result was considered for further investigation. The corrosion current density and corrosion potential were measured on the potentiodynamic curve using the tangent line method. The focal point of tangents at the cathodic polarization curve and anodic polarization curve corresponded to I_{corr} and E_{corr}. Electrochemical impedance spectroscopy (EIS, (Multi Autolab/M204, Metrohm, Zofingen, Switzerland)) was performed at open circuit potential at a frequency ranging from 100 KHz to 0.1 Hz. The impedance data were analyzed using Nyquist and Bode plots. ImageJ software was used to plot the surface roughness morphologies of corroded samples using scanning electron microscope (SEM, model JSM-6390LV) images. The effects of WS_2 concentration, heat treatment, and severe plastic deformation on corrosion properties of AZ91 were analyzed.

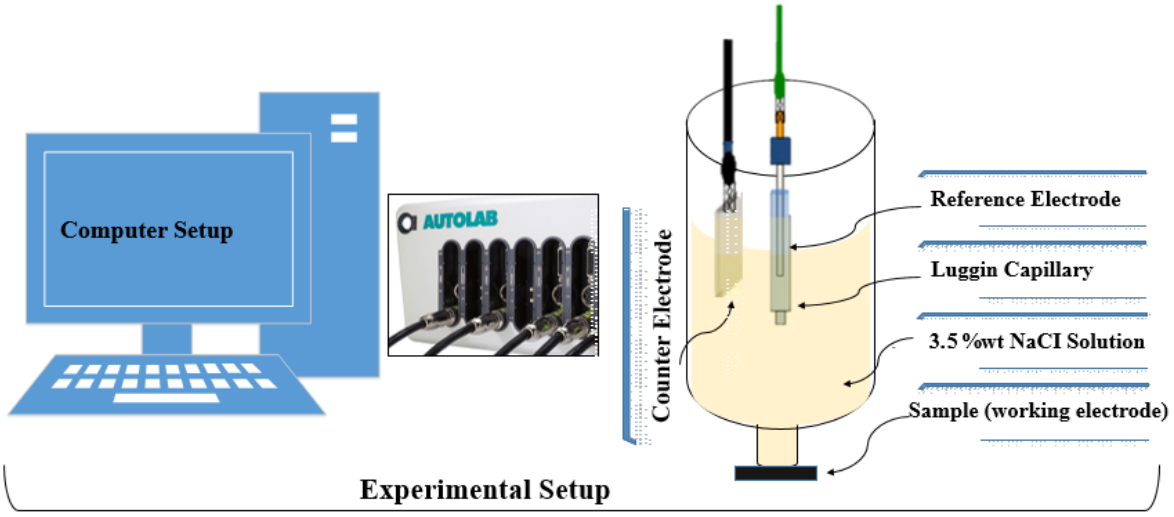

Figure 1. Experimental setup for potentiodynamic polarization.

The degradability of the composites was measured using corrosion rate of composites from Tafel curves using the following relation (Equation (1)) [14].

$$R = 0.129 M_r I_{corr} / n\rho \quad (1)$$

where "M_r" is the relative molecular mass, "I_{corr}" is corrosion current density, "n" is valency and "ρ" is the density of the samples.

3. Results and Discussion

3.1. Potentiodynamic Polarization

Tafel polarization curves of all samples are shown in Figure 2. The samples were immersed in a 3.5 wt% NaCl solution for 1 h to stabilize the OCP prior to the polarization test. The I_{corr} (corrosion current density) and E_{corr} (corrosion potential) are very effective parameters used to analyze the degradation behavior of composites. Generally, a lower corrosion potential and higher I_{corr} indicates a higher degradability of the composites. The electrochemical parameters, including corrosion current density, corrosion potential, degradability, and cathodic and anodic slopes, are summarized in Table 1. The monolithic AZ91 exhibits a −1.55334 mV corrosion potential, which is decreased to −1.5728 mV and −1.56097 mV with the addition of 0.6 wt% and 1 wt% WS_2, respectively, in as-cast condi-

tions (Figure 2a). The decrease in E_{corr} indicates that WS_2 addition has effectively influenced the degradability of AZ91 in as-cast conditions. The decrease in E_{corr} is attributed to the formation of intermetallic compounds, which act as cathodes during micro-galvanic corrosion and enhance the degradation in composites [19,20]. The corrosion potential for 0.6 wt% WS_2/AZ91 was found to be −1.58752 V after two passes of ECAP. The 0.6 wt% WS_2/AZ91 presents a higher corrosion potential in homogenized and SPD conditions (Figure 2). The Tafel curves are summarized in Figure 3 to analyze the effects of homogenization heat treatments and SPD on the degradability of WS_2/AZ91 composites. It can be observed from Figure 3 that monolithic AZ91 exhibits the highest E_{corr} and lowest degradability. It can also be depicted that one-pass AZ91 presents the highest degradation rate and a minimum corrosion potential. The severe plastic deformation and homogenization have a great impact on the degradability of WS^2/AZ91 composites. The monolithic AZ91 and 1 wt% WS_2/AZ91 have almost the same corrosion potential, but heat treatment and SPD have significantly reduced the E_{corr}, and the degradation rate is enhanced. The break in the anodic curve has been observed for composites after severe plastic deformation. The formation of intermetallic compounds and a decrease in grain size after severe plastic deformation lead to micro-galvanic corrosion. Moreover, the refined grains lead to the formation of close-spaced electrochemical batteries of cathodic–anodic regions causing the breaks in the anodic curve.

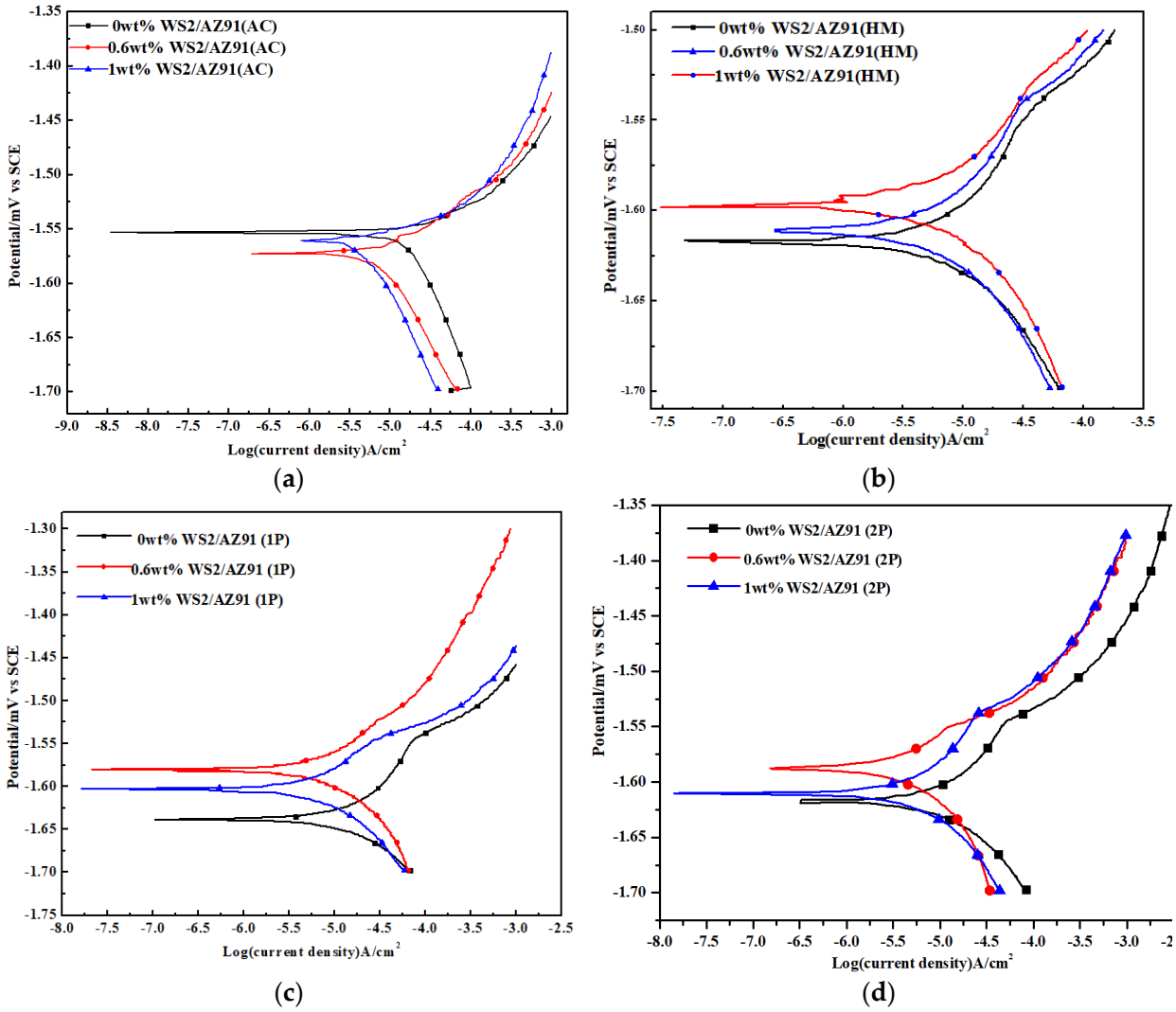

Figure 2. Tafel curves for WS_2/AZ91 composites in (**a**) as-cast, (**b**) homogenized, (**c**) one-pass ECAP, (**d**) two-pass ECAP.

Table 1. Summary of corrosion parameters for WS_2/AZ91 composites.

Composite	Condition	E_{corr} mV)	I_{corr} ($\mu A \cdot cm^{-2}$)	R ($m \cdot a^{-1}$)	Bc ($mV \cdot dec^{-1}$)	Ba ($mV \cdot dec^{-1}$)	Ra (μm)
0 wt% WS2/AZ91	as-cast	−1.55334 ± 0.00011	1.232 ± 0.001	4.09955 ± 0.0005	0.4272 ± 0.0002	0.6321 ± 0.0002	33.90 ± 0.1
0.6 wt% WS2/AZ91		−1.57288 ± 0.00011	1. 954 ± 0.001	4.16262 ± 0.0005	0.4384 ± 0.0002	0.5935 ± 0.0002	34.55 ± 0.1
1 wt% WS2/AZ91		−1.56097 ± 0.00011	1.286 ± 0.001	4.1446 ± 0.0005	0.4394 ± 0.0002	0.5934 ± 0.0002	36.31 ± 0.1
0 wt% WS2/AZ91	Homogenized	−1.61652 ± 0.00008	4.430 ± 0.001	4.51401 ± 0.0005	0.4284 ± 0.0001	0.5493 ± 0.0001	36.95 ± 0.2
0.6 wt% WS2/AZ91		−1.59821 ± 0.00008	3.110 ± 0.001	4.45995 ± 0.0005	0.4566 ± 0.0001	0.6487 ± 0.0001	40.63 ± 0.2
1 wt% WS2/AZ91		−1.61163 ± 0.00008	4.295 ± 0.001	4.5120 ±0.0005	0.5548 ± 0.0001	0.7432 ± 0.0001	41.84 ± 0.2
0 wt% WS2/AZ91	1-pass ECAPed	−1.63849 ± 0.00012	5.80 ± 0.002	4.613 ± 0.0003	0.1779 ± 0.0002	0.3543 ± 0.0002	38.43 ± 0.1
0.6 wt% WS2/AZ91		−1.5799 ± 0.00012	3.237 ± 0.002	4.3248 ± 0.0003	0.3267 ± 0.0002	0.6633 ± 0.0002	41.25 ± 0.1
1 wt% WS2/AZ91		−1.60278 ± 0.00012	3.103 ± 0.002	4.5043 ± 0.0003	0.1890 ± 0.0002	0.4317 ± 0.0002	43.23 ± 0.1
0 wt% WS2/AZ91	2-pass ECAPed	−1.61865 ± 0.00012	3.132 ± 0.002	4.52302 ± 0.0002	0.2126 ± 0.0003	0.6249 ± 0.0003	42.28 ± 0.1
0.6 wt% WS2/AZ91		−1.58752 ± 0.00011	2.219 ± 0.002	4.43292 ± 0.0002	0.2033 ± 0.0003	0.7585 ± 0.0003	42.59 ± 0.1
1 wt% WS2/AZ91		−1.61011 ± 0.00011	3.153 ± 0.002	4.5951 ± 0.0002	0.1995 ± 0.0003	0.5409 ± 0.0003	47.37 ± 0.1

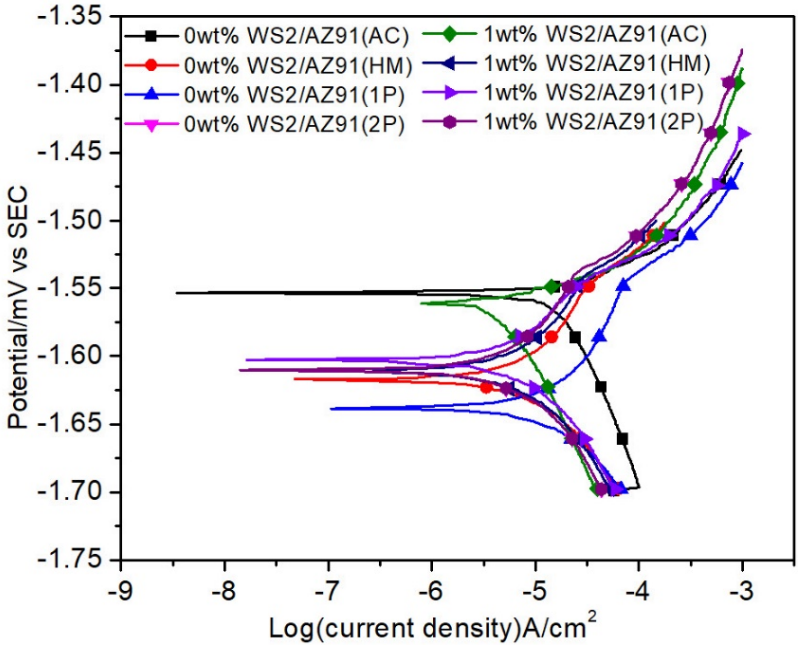

Figure 3. Comparative Tafel curves for WS_2/AZ91 composites.

The I_{corr} decreases with an increase in WS_2 contents in homogenized conditions. This is mainly due to the solid solution heat treatment used to reduce the amount of intermetallic compounds and reduce the corrosion current density [21,22]. Similar polarization curves indicate that all composites have similar degradation behavior. The as-cast and ECAPed composites have nobler Tafel curve slopes than homogenized composites. The corrosion potential is shifted to the nobler potential at the cathodic polarization curve. The SPD and heat treatment enhances the degradability of the composites. The corrosion current density for monolithic AZ91 and 1 wt% WS_2/AZ91 is (1.232 $\mu A \cdot cm^{-2}$) and (1.286 $\mu A \cdot cm^{-2}$) under as-cast conditions, which is increased to (3.132 $\mu A \cdot cm^{-2}$) and (3.153 $\mu A \cdot cm^{-2}$) after two passes of ECAP. The addition of WS_2 contents enhances the degradability of AZ91 under all conditions. The monolithic AZ91 exhibits a corrosion rate (4.5120 $m \cdot a^{-1}$) under as-cast conditions, which is increased to (4.5951 $m \cdot a^{-1}$) for two-pass ECAPed 1 wt% WS_2/AZ9. The degradability of AZ91 is increased under synergic effects of WS_2 contents and SPD. The grain size of the composites is refined after heat treatment and SPD, and more active sites are built up, which leads to an enhanced degradation rate [23].

It can be visualized by Tafel polarization curves (Figure 2) that cathodic polarization curves have regular patterns. A higher corrosion potential will lead to a decrease in corrosion current density. The higher corrosion current will lead to higher corrosion products and an enhanced degradability [24]. Moreover, it can also be seen that the corrosion current densities have decreased with the increase in the number of passes. The higher values of the cathodic constant indicate the occurrence of a cathodic reaction and oxygen reduction reaction.

The degradation in Mg alloys is accompanied by hydrogen evaluation (HE) under anodic polarization in aqueous electrolytes. The reduction in water results in hydrogen evaluation. The phenomenon contradicts standard electrochemical kinetics, whose polarization curves do not present the linear region expected for controlled activation. The most useful aspect of the polarization curve is not the determination of the corrosion rate but relative changes in cathodic and anodic kinetics. The potentiodynamic polarization is the only method used to determine the alloying effects by discriminating the anodic and cathodic kinetics.

The hydrogen evaluation is the cathodic reaction in Mg corrosion that takes place spontaneously under an open circuit. However, when Mg alloys are polarized anodically, a higher degradability and hydrogen evaluation have been observed. The phenomenon

is called the negative difference effect (NDE) and is defined as the difference between HE under open circuit conditions and the rate associated with the hydrogen evaluation reaction (HER) during anodic polarization [25].

According to the univalent theory [25], Mg and its alloys experience a two-step dissolution (a) electrochemical reaction in which a fraction of Mg is dissolved into an Mg^+ solution. (b) Mg^+ reacts with water to form Mg^{2+} and H_2. More Mg^+ ions are produced as a result of the increased dissolution, which consequently increases the hydrogen evaluation.

$$Mg_{(s)} \rightarrow Mg^{+}_{(aq)} + e^{-} \quad (2)$$

$$Mg^{+}_{(aq)} + H_2O \rightarrow Mg^{2+}_{(aq)} + \frac{1}{2}H_2 + OH^{-} \quad (3)$$

The increase in HE is controlled by an increase in the applied current or potential. Mg alloy dissolution proceeds via Mg^{2+}.

The main film formed on the surface of the composites is $Mg(OH)_2$. The possible reaction process for $Mg(OH)_2$ formation is suggested below, which is known as the hydrogen evaluation reaction.

$$2H_2O + 2\,\bar{e} \rightarrow H_2 + 2OH^{-} \quad (4)$$

The Mg^{2+} reacts with OH^- to form $Mg(OH)_2$. The hydrogen generation reactions are increased with the increase in cathodic currents, resulting in an increased local pH at the interface of Mg causing a stronger basicity at a higher hydrogen charging current, which leads to the easy formation of MgO. According to the polarization curves, the cathodic curves present a smaller difference, except for monolithic AZ91.

It can be revealed from the results that the higher hydrogen evaluation is helpful in improving the degradation rate of Mg alloys due to the breakdown of oxide film on the surface. The higher hydrogen evaluation increases the defects in film and deteriorates the protection ability [26].

As the microstructure of the composite is refined, a higher fraction of fine grains is achieved. Additionally, the degradability is increased by accelerating the passivation process and reducing the intensity of the galvanic couple between the grain interior and grain boundary. Therefore, the increase in the number of passes will lead to the formation of more refined grains, which ultimately leads to the formation of closed-spaced electrochemical batteries of the anodic–cathodic region. The increase in the number of passes causes a decrease in grain size, and thus an increase in grain densities and the percentage of higher angle grain boundaries [24]. The difference between the rate of anodic and cathodic reactions is expected to alter significantly, which leads to a more uniform attack and a higher rate of degradation.

The addition of WS_2 to AZ91 alloy appears to decrease the corrosion potential in the more negative direction, which could be due to an increase in the cathodic reaction. The degradation rate can be estimated by the corrosion current and it is indicated from Table 1 that the I_{corr} of as-cast samples is smaller, which means a lower degradability. The increase in I_{corr} could be due to the galvanic coupling between secondary phases and the Mg matrix where the Mg matrix and secondary phases can act as an anode and cathode, respectively. After the heat treatment, I_{corr} is significantly increased, which can be explained by changes in the distribution of WS_2 as secondary phases in the Mg matrix. It can be noted from Table 1 that Tafel anodic and cathodic slopes are changed with the increase in WS_2 concentration, homogenization, and ECAP processes. The synergic effects of WS_2 concentration and SPD affect the anodic and cathodic reactions, causing an increased degradation rate.

3.2. Electrochemical Impedance Spectroscopy

The Nyquist plots for all samples are presented in Figure 4. The results for monolithic AZ91 and 1 wt% WS_2/AZ91 are also separately plotted in Figure 5 to investigate the comparative effects of heat treatment and SPD. The monolithic AZ91 exhibits the largest capacitive curve diameter in as-cast conditions, and the diameter is reduced when WS_2 is

added to the matrix. The addition of reinforcement (WS_2) increases the capacitive curve diameter in homogenized conditions. The diameter of composites with 0 wt% and 0.6 wt% is increased drastically in homogenized conditions compared with as-cast conditions. However, under the SPD conditions, 0.6 wt% WS_2/AZ91 represents the maximum diameter of impedance curves. The larger the semicircle diameter, the higher the corrosion resistance. The smaller semicircle indicates the higher degradability of the composites. The sudden drop in the semicircle of 0.6 wt% WS_2/AZ91 after one pass of ECAP may be due to irregularities on the surface [27]. The larger diameter curves indicate the presence of an improved corrosion resistance and lower degradability [28]. The results are in good agreement with Tafel curves. As indicated in Figure 5, the monolithic as-cast AZ91 presents the largest capacitive diameter, and, after one pass of ECAP, it has a minimum diameter. The corrosion results are also in agreement with the mechanical properties determined by the author previously [8,18]. The decrease in grain size leads to a higher yield strength and enhanced degradation rate. The similar shape of the capacitive curves indicates that corrosion behavior is only due to charge transfer.

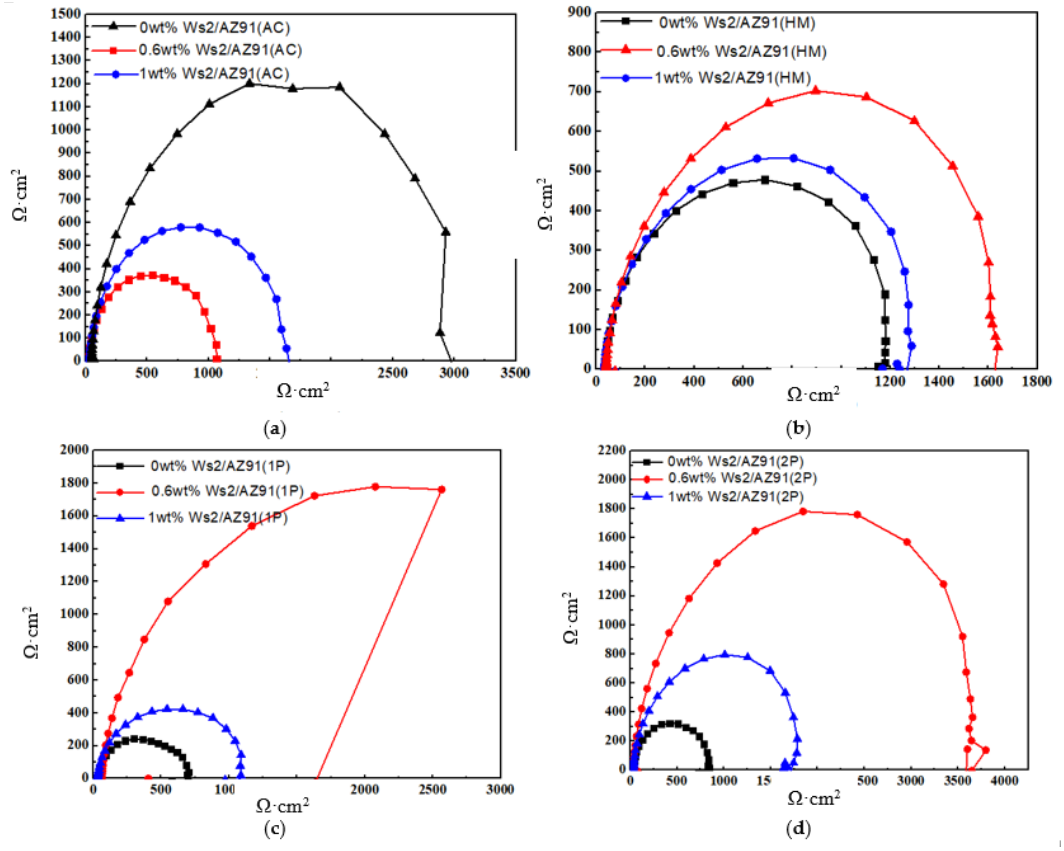

Figure 4. Nyquist plots for WS_2/AZ91 composites in (**a**) as-cast, (**b**) homogenized, (**c**) one-pass ECAP, (**d**) two-pass ECAP.

The Bode diagrams are presented in Figure 6 for WS_2/AZ91 composites under all conditions. The enlarged view is also presented to understand the peak diversion behavior of the samples and to evaluate the electrode reactions effectively. The Bode plots give a better insight into the passivity response as a charge transfer and diffusion phenomenon, as it was mentioned earlier that as-cast samples exhibit a better corrosion response and corrosion protective ability. Every composite presents a steady drop in the phase angle, which confirms the presence of the passivation layer, which also decreases the protective properties with respect to time and frequency. The greater and highest phase angle reveals a high electrochemical resistance, which further shows the high-density oxide film establishment. The highest phase angle at the knee has been observed in 1 wt% WS_2/AZ91 in

as-cast (68°) and homogenized conditions (65°). The monolithic AZ91 experience phase angle at the knee is 64°, 63°, 52°, and 62° for AC (as-cast), HM (homogenized), 1EACP (one pass), and 2EACP (two passes), respectively, whereas composites with 1 wt% WS_2 have a phase angle of 70°, 69°, 65°, and 64° for AC, HM, 1 EACP, and 2EACP, respectively [29]. The composites with 1 wt% WS_2 show a sharper drop in the phase angle in all conditions compared to monolithic AZ91 (Figure 7). The high-frequency loop is attributed to the charge transfer reaction between the metal surface and corrosive medium, which can be described by the charge transfer resistance and constant phase element [30]. The low frequency is attributed to mass transport in the solid solution, such as the diffusion of ions through the oxide film, which can be described by the film capacity and film resistance [27].

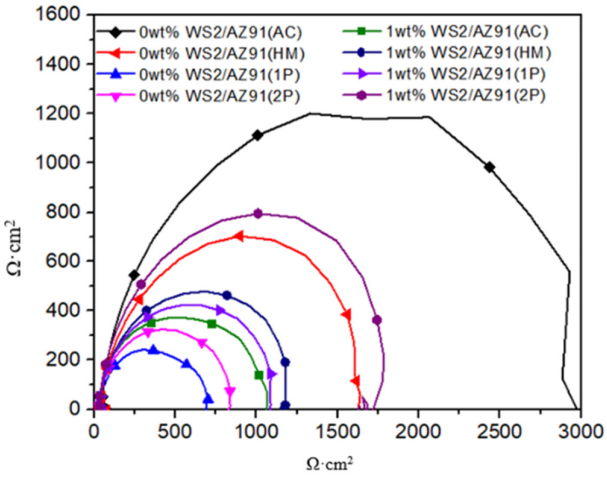

Figure 5. Comparative Nyquist plots for WS2/AZ91 composites.

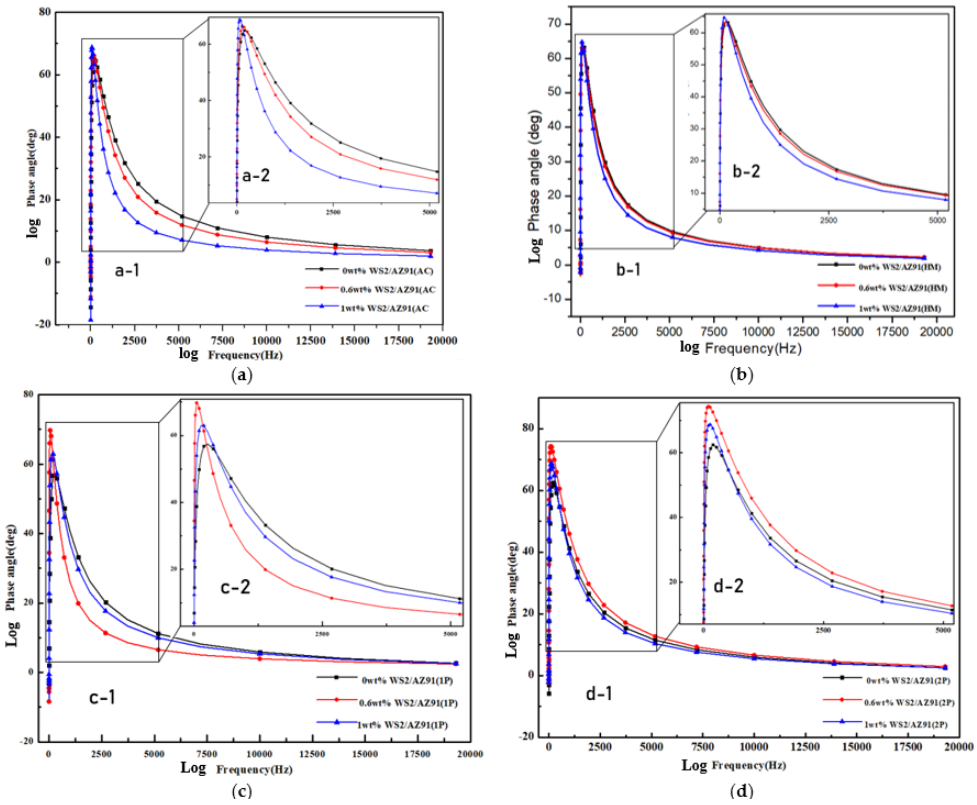

Figure 6. Bode diagrams for WS_2/AZ91 composites in (**a**) as-cast, (**b**) homogenized, (**c**) one-pass ECAP, (**d**) two-pass ECAP.

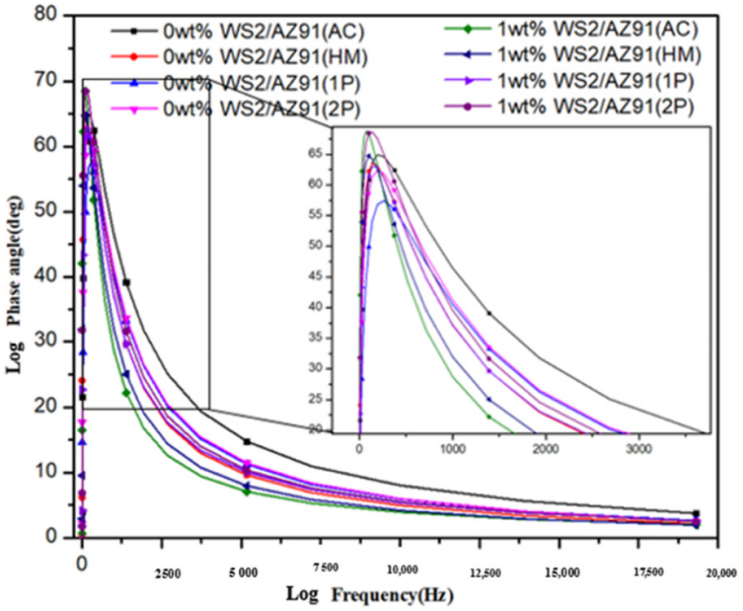

Figure 7. Comparative Bode diagrams for WS_2/AZ91 composites.

3.3. Microstructural Characterization

ImageJ was used to plot the surface roughness of SEM images to investigate the materials removed by corrosion. The surface roughness profiles generated by SEM images are given in Figure 8, and the corresponding roughness values are given in Table 1.

The microstructure is the decisive factor in analyzing the degradation behavior of the composites. A homogeneous microstructure with micron-sized grains is beneficial for a higher degradability. The SPD along with homogenization increased the grain density [21]. The degree of porosity and grain density plays an important role in determining corrosion behavior. The presence of higher porosities significantly improves the degradability. On the other hand, SPD induces more active sites, which leads to higher current densities. The degree of plastic deformation significantly affects the microstructure, precipitates, and degradation behavior of the composites [14,31].

It has been investigated by Mohammed Ibrahim et al. [32] that the degradation rate is inversely related to the square root of the grain size as given below in Equation (5).

$$R = A - Bd^{-1/2} \quad (5)$$

where R, A, and B are the corrosion rate (degradability) and constants related to materials and electrolyte concentration. It has been observed that the degradability of the composites is dependent on the grain size and secondary phases present in the microstructure. The corrosion potential is the open circuit potential where both cathodic and anodic reactions are in equilibrium, and a lower corrosion potential will have a better degradability. The corrosion potential of as-cast composites was found to be nobler than homogenized and ECAPed composites, which indicates their active behavior in the NaCl solution. The relatively more positive corrosion potential of ECAPed composites is presumed to be due to the presence of secondary phases that increase the potential during equilibrium. The as-cast samples showed a higher corrosion potential compared to the respective homogenized samples. The heat-treated samples with a lower porosity and a homogeneous microstructure with a fine and continuous distribution of secondary phases could be the reason for the higher degradation rate. The Nyquist exhibit similar shapes, except for their diameters, which indicate that all alloys have similar corrosion mechanisms but different degradation rates. The imperfection in the shape of the semicircle is due to surface roughness [17,33].

The microstructure of AZ91 mainly consists of the α (primarily Mg) and β-($Mg_{17}Al_{12}$) phases. The β-phases are present in form of a network and distributed around α- Mg.

For detailed information, please refer to our previous research [8]. The increase in WS_2 contents refined the grain size and lamellar-shaped β-phases. The β-phases have a significant influence on the corrosion behavior of the Mg alloys. The β-phase possesses a higher positive corrosion potential and lower anodic kinetics in lower anodic polarization. Hydrogen can permeate into the alloys and gather to initiate the hydrogen embrittlement phenomenon [34]. This causes cracks in β-phases and initiates stress corrosion cracking in AZ91 alloys. The decrease in β-phases is also a reason for the increase in the corrosion rate in composites with higher contents of WS_2.

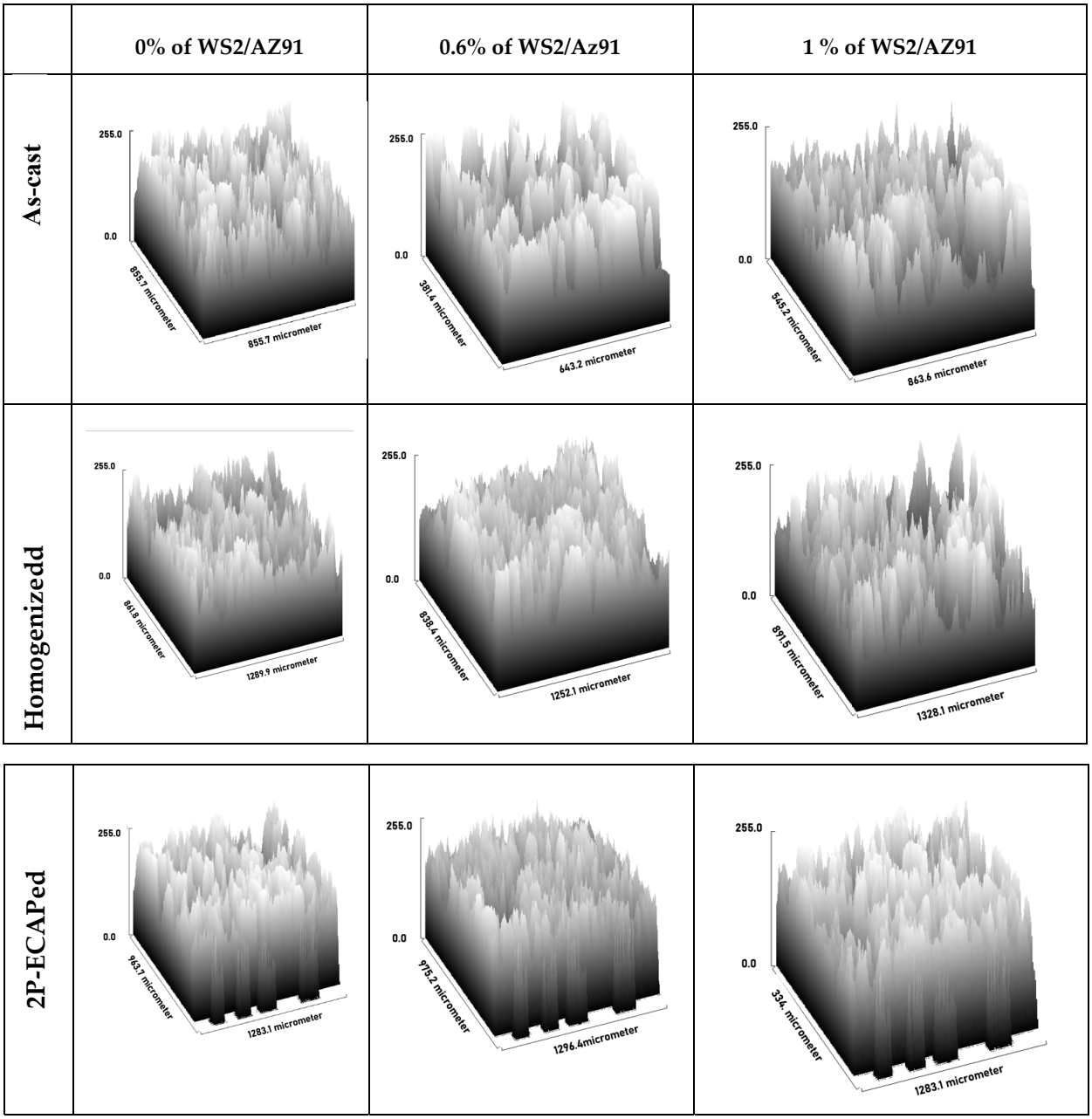

Figure 8. Surface roughness generated by SEM images of corroded WS_2/AZ91 samples.

The surface roughness of corroded samples was measured to analyze the materials lost. Higher surface roughness values indicate a higher number of materials removed. It can be observed that monolithic AZ91 indicates a minimum surface roughness (33.90 μm), and two-pass ECAPed 1 wt% WS_2/AZ91 represents a maximum surface roughness (47.37 μm). The surface roughness indicates that the materials removed by corrosion is the maximum

in two-pass ECAPed 1 wt% WS_2/AZ91. The degradability of the composites has been correlated with surface roughness produced after corrosion experiments [27]. Higher degradation will lead to higher corrosion products on the surface, which will consequently cause a higher surface roughness. The results are in good agreement with the XRD pattern available (Figure 9). The two-pass ECAPed 0.6 wt% WS_2/AZ91 represents relatively fewer material removals compared with other composites.

The corrosion products were investigated using XRD analysis. The XRD patterns of corroded samples are presented in Figure 9. The presence of MgO (JCPDS card No. 4−0829) and $Mg(OH)_2$ (JCPDS card: 75–1527) peaks in XRD patterns indicate the corrosion products. One peak of magnesium oxide and one peak of magnesium hydroxide are present in the XRD pattern. As-cast samples have minimum peak intensities of MgO and $Mg(OH)_2$. Higher peak intensities are found in 2P samples. The magnesium oxide and hydroxide peaks are increased with the increase in WS_2 contents in as-cast and homogenized conditions. The improved grain structure and reduced internal stresses resulting from heat treatment yielded a negative potential and deteriorated the corrosion resistance [14]. The two-pass ECAP also presents higher peaks of corrosion products with an increase in WS_2 concentration, indicating that the degradation rate increases with grain refinement. The smaller the grain size, the large the degradation rate. The pits are grown on the surface and the continuous process of propagation causes uniform corrosion. A higher number of materials lost will lead to enhanced corrosion products. The results are in good agreement with Tafel curves and Nyquist plots.

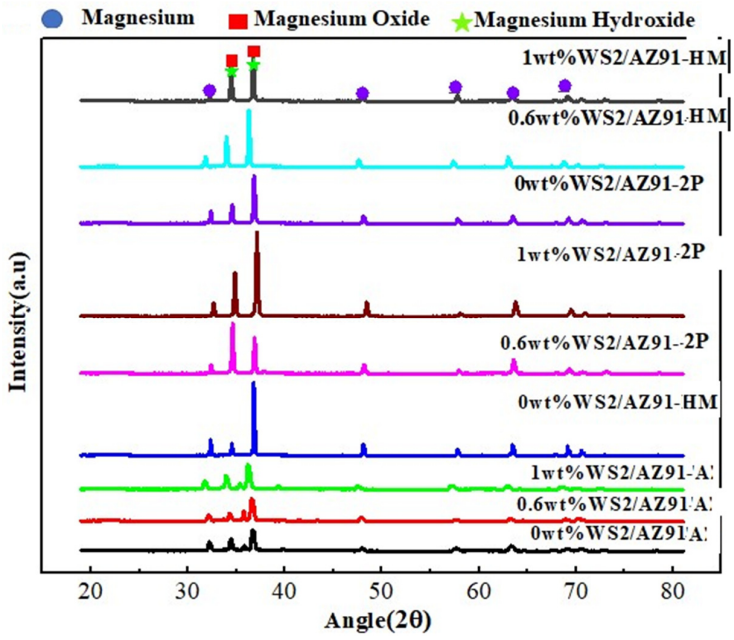

Figure 9. XRD analysis of corroded WS_2/AZ91 composites.

4. Conclusions

In summary, AZ91 reinforced with WS_2 was manufactured using the stir casting method. The degradation behavior of as-casted and ECAPed composites was investigated in a 3.5 wt% NaCl solution in a three-electrode cell system. The results can be concluded as below:

1. The monolithic AZ91 exhibits a maximum corrosion resistance and degradation rate (4.5120 $m{\cdot}a^{-1}$) in as-cast conditions.
2. Two-pass ECAPed 1 wt% WS_2/AZ91 has a corrosion potential of (−1.6101 mV) and a corrosion rate of (4.5951 $m{\cdot}a^{-1}$); however, a minimum corrosion potential (−1.63849 mV) and maximum degradation rate (4.613 $m{\cdot}a^{-1}$) was recorded for one-pass ECAPed 0 wt% WS_2/AZ91.

3. All composites exhibit similar Tafel curves, which indicates that similar corrosion behavior has taken place in all samples.
4. The degradability of AZ91 is increased in all conditions under the synergic effect of WS_2 and severe plastic deformation.
5. The passive layers of oxide and hydroxide film were established on the corroded surface of all composites

Author Contributions: Data curation, A.A.; Funding acquisition, S.-J.H.; Investigation, A.A.; Resources, S.-J.H.; Supervision, S.-J.H.; Writing—original draft, A.A. All authors have read and agreed to the published version of the manuscript.

Funding: This research received no external funding.

Institutional Review Board Statement: Not applicable.

Informed Consent Statement: Not applicable.

Data Availability Statement: Not applicable.

Conflicts of Interest: The authors declare no conflict of interest.

References

1. Sundaresan, R.; Froes, F.H. Mechanical Alloying in the Titanium-Magnesium System. *Key Eng. Mater.* **1991**, *29–31*, 199–206. [CrossRef]
2. Rashad, M.; Pan, F.; Liu, Y.; Chen, X.; Lin, H.; Pan, R.; Asif, M.; She, J. High Temperature Formability of Graphene Nanoplatelets-AZ31 Composites Fabricated by Stir-Casting Method. *J. Magnes. Alloy.* **2016**, *4*, 270–277. [CrossRef]
3. Mediaswanti, K.; Wen, C.; Ivanova, E.P.; Berndt, C.C.; Malherbe, F.; Thi, V.; Pham, V.T.H.; Wang, J. A Review on Bioactive Porous Metallic Biomaterials. *J. Biomim. Biomater. Tissue Eng.* **2013**, *18*, 1–8. [CrossRef]
4. Wang, X.J.; Hu, X.S.; Liu, W.Q.; Du, J.F.; Wu, K.; Huang, Y.D.; Zheng, M.Y. Ageing Behavior of As-Cast SiCp/AZ91 Mg Matrix Composites. *Mater. Sci. Eng. A* **2017**, *682*, 491–500. [CrossRef]
5. Yeganeh, M.; Mohammadi, N. Superhydrophobic Surface of Mg Alloys: A Review. *J. Magnes. Alloy.* **2018**, *6*, 59–70. [CrossRef]
6. Luo, A.A. Magnesium Casting Technology for Structural Applications. *J. Magnes. Alloy.* **2013**, *1*, 2–22. [CrossRef]
7. Kumar, D.; Thakur, L. Recent Studies on the Fabrication of Magnesium Based Metal Matrix Nano-Composites by Using Ultrasonic Stir Casting Technique—A Review. *Mater. Sci. Forum* **2019**, *969*, 889–894. [CrossRef]
8. Huang, S.-J.; Abbas, A. Effects of Tungsten Disulfide on Microstructure and Mechanical Properties of AZ91 Magnesium Alloy Manufactured by Stir Casting. *J. Alloys Compd.* **2020**, *817*, 153321. [CrossRef]
9. Abbas, A.; Huang, S.-J. Qualitative and Quantitative Investigation of As-Cast and Aged CNT/AZ31 Metal Matrix Composites. *JOM* **2020**, *72*, 2272–2282. [CrossRef]
10. Abbas, A.; Huang, S.-J. ECAP Effects on Microstructure and Mechanical Behavior of Annealed WS2/AZ91 Metal Matrix Composite. *J. Alloys Compd.* **2020**, *835*, 155466. [CrossRef]
11. Yu, W.; Wang, X.; Zhao, H.; Ding, C.; Huang, Z.; Zhai, H.; Guo, Z.; Xiong, S. Microstructure, Mechanical Properties and Fracture Mechanism of Ti_2AlC Reinforced AZ91D Composites Fabricated by Stir Casting. *J. Alloys Compd.* **2017**, *702*, 199–208. [CrossRef]
12. Zhang, Y.; Zhang, W.; Li, B.; Ren, H.; Qi, Y.; Zhao, D. Effects of Milling Duration on Electrochemical Hydrogen Storage Behavior of As-Milled Mg–Ce–Ni–Al-Based Alloys for Use in Ni-Metal Hydride Batteries. *J. Phys. Chem. Solids* **2019**, *133*, 178–186. [CrossRef]
13. Kim, W.J.; Jeong, H.G.; Jeong, H.T. Achieving High Strength and High Ductility in Magnesium Alloys Using Severe Plastic Deformation Combined with Low-Temperature Aging. *Scr. Mater.* **2009**, *61*, 1040–1043. [CrossRef]
14. Bin, B.S.J.; Tan, Y.T.; Fong, K.S.; Tan, M.J. Effect of Severe Plastic Deformation and Post-Annealing on the Mechanical Properties and Bio-Corrosion Rate of AZ31 Magnesium Alloy. *Procedia Eng.* **2017**, *207*, 1475–1480. [CrossRef]
15. Ralston, K.D.; Birbilis, N. Effect of Grain Size on Corrosion: A Review. *Corrosion* **2010**, *66*, 075005–075013. [CrossRef]
16. Huot, J. Nanocrystalline Metal Hydrides Obtained by Severe Plastic Deformations. *Metals* **2012**, *2*, 22–40. [CrossRef]
17. Hamu, G.B.; Eliezer, D.; Wagner, L. The Relation between Severe Plastic Deformation Microstructure and Corrosion Behavior of AZ31 Magnesium Alloy. *J. Alloys Compd.* **2009**, *468*, 222–229. [CrossRef]
18. Abbas, A.; Huang, S.-J. Investigation of Severe Plastic Deformation Effects on Microstructure and Mechanical Properties of WS2/AZ91 Magnesium Metal Matrix Composites. *Mater. Sci. Eng. A* **2020**, *780*, 139211. [CrossRef]
19. Mehrian, S.S.M.; Rahsepar, M.; Khodabakhshi, F.; Gerlich, A.P. Effects of Friction Stir Processing on the Microstructure, Mechanical and Corrosion Behaviors of an Aluminum-Magnesium Alloy. *Surf. Coat. Technol.* **2021**, *405*, 126647. [CrossRef]
20. Liu, H.; Yan, Y.; Wu, X.; Fang, H.; Chu, X.; Huang, J.; Zhang, J.; Song, J.; Yu, K. Effects of Al and Sn on Microstructure, Corrosion Behavior and Electrochemical Performance of Mg–Al-Based Anodes for Magnesium-Air Batteries. *J. Alloys Compd.* **2021**, *859*, 157755. [CrossRef]
21. Liu, X.; Shan, D.; Song, Y.; Han, E. Effects of Heat Treatment on Corrosion Behaviors of Mg-3Zn Magnesium Alloy. *Trans. Nonferrous Met. Soc. China* **2010**, *20*, 1345–1350. [CrossRef]

22. Abbas, A.; Rajagopal, V.; Huang, S.-J. Magnesium Metal Matrix Composites and Their Applications. In *Magnesium Alloys*; IntechOpen: London, UK, 2021.
23. Li, Z.; Peng, Z.; Qiu, Y.; Qi, K.; Chen, Z.; Guo, X. Study on Heat Treatment to Improve the Microstructure and Corrosion Behavior of ZK60 Magnesium Alloy. *J. Mater. Res. Technol.* **2020**, *9*, 11201–11219. [CrossRef]
24. Liu, Q.; Chen, G.; Zeng, S.; Zhang, S.; Long, F.; Shi, Q. The Corrosion Behavior of Mg-9Al-XRE Magnesium Alloys Modified by Friction Stir Processing. *J. Alloys Compd.* **2021**, *851*, 156835. [CrossRef]
25. Esmaily, M.; Svensson, J.E.; Fajardo, S.; Birbilis, N.; Frankel, G.S.; Virtanen, S.; Arrabal, R.; Thomas, S.; Johansson, L.G. Fundamentals and Advances in Magnesium Alloy Corrosion. *Prog. Mater. Sci.* **2017**, *89*, 92–193. [CrossRef]
26. Song, Y.; Han, E.-H.; Dong, K.; Shan, D.; Yim, C.D.; You, B.S. Effect of Hydrogen on the Corrosion Behavior of the Mg–XZn Alloys. *J. Magnes. Alloy.* **2014**, *2*, 208–213. [CrossRef]
27. Xu, F.; Luo, L.; Xiong, L.; Liu, Y. Microstructure and Corrosion Behavior of ALD Al_2O_3 Film on AZ31 Magnesium Alloy with Different Surface Roughness. *J. Magnes. Alloy.* **2020**, *8*, 480–492. [CrossRef]
28. García-Rodríguez, S.; Torres, B.; Pulido-González, N.; Otero, E.; Rams, J. Corrosion Behavior of 316L Stainless Steel Coatings on ZE41 Magnesium Alloy in Chloride Environments. *Surf. Coat. Technol.* **2019**, *378*, 124994. [CrossRef]
29. Mahdavian, M.; Attar, M.M. Another Approach in Analysis of Paint Coatings with EIS Measurement: Phase Angle at High Frequencies. *Corros. Sci.* **2006**, *48*, 4152–4157. [CrossRef]
30. Xu, Z.; Eduok, U.; Tiamiyu, A.A.; Szpunar, J. Anodic Dissolution Pattern of Magnesium Alloy in Different Media: Effects of Solution Treatment on Its Microstructure and Corrosion Behaviour. *Eng. Fail. Anal.* **2020**, *107*, 104234. [CrossRef]
31. Vaughan, M.W.; Karayan, A.I.; Srivastava, A.; Mansoor, B.; Seitz, J.M.; Eifler, R.; Karaman, I.; Castaneda, H.; Maier, H.J. The Effects of Severe Plastic Deformation on the Mechanical and Corrosion Characteristics of a Bioresorbable Mg-ZKQX6000 Alloy. *Mater. Sci. Eng. C* **2020**, *115*, 111130. [CrossRef]
32. Jamesh, M.I.; Wu, G.; Zhao, Y.; Jin, W.; McKenzie, D.R.; Bilek, M.M.M.; Chu, P.K. Effects of Zirconium and Nitrogen Plasma Immersion Ion Implantation on the Electrochemical Corrosion Behavior of Mg–Y–RE Alloy in Simulated Body Fluid and Cell Culture Medium. *Corros. Sci.* **2014**, *86*, 239–251. [CrossRef]
33. Sajjad, U.; Abbas, A.; Sadeghianjahromi, A.; Abbas, N.; Liaw, J.-S.; Wang, C.-C. Enhancing Corrosion Resistance of Al 5050 Alloy Based on Surface Roughness and Its Fabrication Methods; an Experimental Investigation. *J. Mater. Res. Technol.* **2021**, *11*, 1859–1867. [CrossRef]
34. Yang, Y.; Xiong, X.; Chen, J.; Peng, X.; Chen, D.; Pan, F. Research Advances in Magnesium and Magnesium Alloys Worldwide in 2020. *J. Magnes. Alloy.* **2021**, *9*, 705–747. [CrossRef]